Eddy Acceleration and Decay Driven by Internal Tides

CALLUM J. SHAKESPEARE[a,b]

[a] *Research School of Earth Sciences, The Australian National University, Canberra, Australian Capital Territory, Australia*
[b] *ARC Centre of Excellence for Climate Extremes, The Australian National University, Canberra, Australia*

(Manuscript received 5 July 2023, in final form 26 August 2023, accepted 29 September 2023)

ABSTRACT: Recent observations and numerical simulations have demonstrated the potential for significant interactions between mesoscale eddies and smaller-scale tidally generated internal waves—also known as internal tides. Here, we develop a simple theoretical model that predicts the one-way upscale transfer of energy from internal tides to mesoscale eddies through a critical level mechanism. We find that—in the presence of a critical level—the internal tide energy flux into an eddy is partitioned according to the wave frequency Ω and local inertial frequency f: a fraction of $1 - f/\Omega$ is transferred to the eddy kinetic energy, while the remainder is viscously dissipated or supports mixing. These predictions are validated by comparison with a suite of numerical simulations. The simulations further show that the wave-driven energization of the eddies also accelerates the onset of hydrodynamical instabilities and the breakdown of the eddies, thereby increasing eddy kinetic energy, but reducing eddy lifetimes. Our estimates suggest that in regions of the ocean with both significant eddy fields and internal tides—such as parts of the Gulf Stream and Antarctic Circumpolar Current—the critical level effect could drive a $\sim$10% month^{-1} increase in the kinetic energy of a typical eddy. Our results provide a basis for parameterizing internal tide–eddy interactions in global ocean models where they are currently unrepresented.

KEYWORDS: Eddies; Energy transport; Internal waves; Mesoscale processes

1. Introduction

Internal tides, or tidally generated internal waves, inject significant energy ($\sim$1 TW) into the global oceans (Wunsch and Ferrari 2004). The majority of this energy cascades to smaller scales through wave–wave interactions and wave breaking, driving the mixing that sustains the diapycnal transport of mass and tracers. However, internal tides also interact with the ocean mesoscale circulation—in particular, eddies and jets—through so-called "wave-to-mean" interactions (e.g., Müller 1976). These energy exchanges can be in either direction and represent a significant uncertainty in the global internal wave energy budget (Ferrari and Wunsch 2009). A positive wave-to-mean transfer (i.e., energy from waves to eddies) is important because it both reduces the energy available to support mixing and alters its distribution, as well as enhancing the energy of the eddying flow. This enhancement, in turn, increases eddy heat and mass fluxes, which alter global circulation and climate (e.g., Rintoul 2018). Understanding such effects is increasingly vital in the context of significant and largely unexplained changes in the global eddy field in recent decades (Martínez-Moreno et al. 2021).

The concept of wave-to-mean energy exchanges is relatively simple. An internal wave carries with it a certain amount of momentum (or more correctly, "pseudomomentum"; McIntyre 1981) in its direction of propagation which—if the wave is forced to dissipate or otherwise decay—is deposited into the flow, since momentum must be conserved even if the wave vanishes. The product of this momentum flux divergence (i.e., a force $\mathbf{F}$) and the local flow velocity $\mathbf{u}$ is the work done on the flow, $W = \mathbf{F} \cdot \mathbf{u}$—also known as the wave-to-mean conversion. It follows that if the wave field is isotropic and wave dissipation does not depend on the direction of wave propagation, then the net force $\mathbf{F}$ and wave-to-mean conversion will be zero. Thus, to obtain a net wave-to-mean conversion requires something that breaks the symmetry of the wave field, either at generation or termination (or both). Previous work by Shakespeare and Hogg (2019) and Shakespeare (2020) focused on the generation side of the problem, showing how the presence of a time-mean flow at the ocean bottom—in addition to an oscillatory tidal flow—gives rise to a net (spatial mean) force capable of driving upper ocean circulation. However, the simulations presented in Shakespeare and Hogg (2019) also suggested an influence from asymmetric wave dissipation; in particular, it was proposed that internal tides dissipate preferentially when propagating with the local flow, and thereby accelerating ($W = \mathbf{F} \cdot \mathbf{u} > 0$) the simulated eddy field. Unfortunately, the complexity of their simulations did not allow the eddy acceleration effect to be disentangled from other wave processes. Here, we study this effect in isolation.

The mechanism of eddy acceleration suggested by Shakespeare and Hogg (2019) relies on a phenomenon known as critical (or inertial) levels (e.g., Jones 1967; Booker and Bretherton 1967; Xie and Vanneste 2017), a schematic of which is shown in Fig. 1. For an internal tide, a critical level occurs when the wave propagates up into a surface-intensified flow (e.g., an eddy) in the same direction as the wave propagation. The flow acts to increase the vertical wavenumber until at some point—if the velocity becomes large enough—the wavenumber (and vertical shear of the wave) approaches infinity, vertical propagation stalls, and the wave decays through breaking or shear instability. In contrast, internal tides propagating against the flow experience a reduced vertical wavenumber and shear, and thus minimal (if any) wave decay. Critical levels therefore provide a mechanism for the preferential (or even exclusive) decay of internal tides propagating in the direction of the flow. Muench and Kunze (2000) suggested that a

Corresponding author: Callum J. Shakespeare, callum.shakespeare@anu.edu.au

DOI: 10.1175/JPO-D-23-0127.1

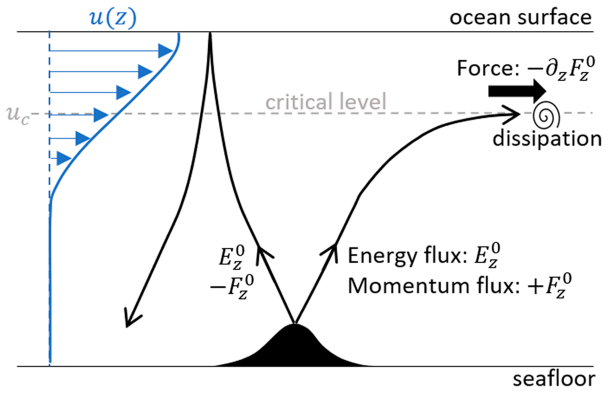

FIG. 1. Schematic of critical level dynamics for internal tides propagating upward into a surface-intensified (2D) flow. The internal tides are generated symmetrically such that waves going in opposite directions have equal energy fluxes E_z^0 and equal and opposite vertical fluxes of horizontal momentum F_z^0 (Shakespeare 2020). The wave traveling in the direction of the flow (blue vectors) experiences an increase in vertical wavenumber m until $m \to \infty$ at the critical level, where $u(z) = u_c = (\Omega - f)/k$ for wave frequency Ω, inertial frequency f, and horizontal wavenumber k. At the critical level, the wave is forced to decay and deposit its momentum into the flow resulting in a force $-\partial_z F_z^0$. The wave energy can either be dissipated or transferred to the surface flow. The wave traveling opposite to the direction of the flow does not encounter a critical level; instead, it reflects back out of the flow with no change in energy or momentum. As such, there exists a net force that accelerates the surface flow.

similar mechanism—but due to the background Garrett–Munk internal wave field (Garrett and Munk 1975) rather than internal tides specifically—is responsible for maintaining the equatorial deep jets. The same basic mechanism of preferential wave dissipation has also been studied in the atmospheric literature in the context of the quasi-biennial oscillation (Plumb 1977; Plumb and McEwan 1978; Baldwin et al. 2001).

Recent observations have highlighted the potential for significant internal-tide-to-mean energy exchanges in the Southern Ocean. Cusack et al. (2020) deployed a mooring array over an abyssal hill in the Scotia Sea, a region with both an intense eddy field and significant semidiurnal internal tides. They found that eddies gain energy from the internal wave field at over 2 mW m^{-2}, with around 50% of this exchange occurring at the tidal frequency. As such, their results suggest that interactions with internal tides may play a significant role in modifying the Southern Ocean mesoscale eddy field. Motivated by the observations of Cusack et al. (2020) and the numerical simulations of Shakespeare and Hogg (2019), here we seek to investigate the influence of internal tides generated at abyssal hills on the energy and life cycle of mesoscale eddies. We pursue this topic with a view to building a parameterization of internal tide–eddy interactions for global ocean models where internal tides are currently unresolved and unrepresented.

The paper is laid out as follows. In section 2, we develop a simple theory for the acceleration of axisymmetric eddies by internal tides, and the partitioning of energy between wave-to-mean conversion and wave dissipation. In section 3, we then evaluate the theory using a suite of idealized numerical simulations. Last, in section 4, we discuss the implications of our results for the mesoscale eddy field and the pathway toward parameterization of these effects in global ocean models.

2. Theory

Here, we consider the scenario shown in Fig. 2 where an isotropic field of internal tides generated by tidal flow over abyssal hills propagates up into a axisymmetric, surface-intensified

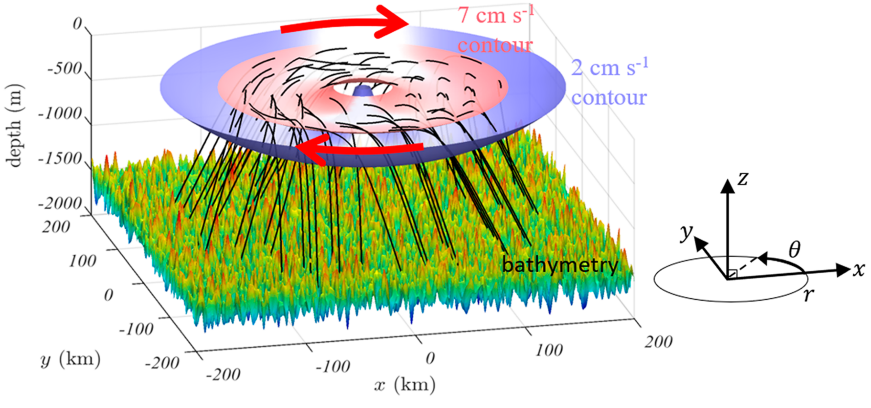

FIG. 2. Schematic of eddy acceleration due to internal tides generated at abyssal hill topography terminating at critical levels within the eddy. Only ray paths (black lines) for internal tides that encounter a critical level are shown, which on average occur equally for waves traveling in all directions, but locally only for waves traveling with the eddy circulation. Isosurfaces of eddy flow speed at 2 and 7 cm s^{-1} are shown. Red arrows indicate the sense of the circulation of (and force on) the eddy. Internal wave ray paths are calculated using parameter values for case 1 (see Table 1) and a horizontal wavenumber magnitude of $|\mathbf{k}_h| = 2\pi/10$ km.

mesoscale eddy.[1] The waves propagate upward until they encounter a critical level, at which point their vertical wavenumber becomes infinite and their vertical propagation stalls. Example ray paths for these internal waves are shown by black lines on the figure. Some waves (not shown) may reflect back and forth between the surface and seafloor, and be deflected through the eddy multiple times, before encountering this critical level. However, once a critical level in encountered, any momentum carried by the waves must be transferred to the flow at that location. The critical level is defined by the intrinsic frequency ω approaching inertial frequency f, since for $\omega < f$, no waves are able to exist. Thus, for a critical level,

$$\omega = \Omega - \mathbf{k}\cdot\mathbf{u} \to f, \tag{1}$$

for tidal frequency Ω and wavevector $\mathbf{k}$; the term $\mathbf{k}\cdot\mathbf{u}$ is usually called the Doppler shift. In the present situation, there is no vertical flow, and hence, $\mathbf{k}\cdot\mathbf{u} = \mathbf{k}_h\cdot\mathbf{u}$, where $\mathbf{k}_h$ is the horizontal wavevector. In the hydrostatic limit, the vertical wavenumber is $m = N|\mathbf{k}_h|/\sqrt{\omega^2 - f^2}$, which approaches infinity as $\omega \to f$.

The assumed axisymmetry of the eddy makes it convenient to use cylindrical coordinates as indicated in Fig. 2 (radius r from the eddy center, angle θ anticlockwise from the + x axis, and depth z) whereby the eddy flow is entirely in the azimuthal θ direction. Therefore, in cylindrical coordinates, $\mathbf{k}_h = (k_r, k_\theta, 0)$ and Eq. (1) reduces to $k_\theta u_\theta = \Omega - f$. Thus, only waves propagating *with* the flow ($k_\theta > 0$) will encounter a critical level, implying that a force is applied in the direction of the flow, and therefore, the eddy will be accelerated by this effect (as indicated by the arrows on Fig. 2). The critical level is independent of the radial wavenumber k_r, and therefore, for an isotropic wavefield, we anticipate an equal distribution of positive and negative k_r in the "critical" waves and therefore zero net *radial* momentum flux—this assumption will prove important in formulating the equations below.

We now seek to calculate the acceleration of the eddy through the critical level mechanism. Given the above assumptions, we can write the azimuthal-mean (denoted by an overbar) momentum balance of the eddy as

$$\frac{\partial \overline{u}_\theta}{\partial t} = -\frac{\partial F_z}{\partial z} \tag{2}$$

in the azimuthal direction, and geostrophic balance

$$f\overline{u}_\theta = \frac{\partial \overline{p}}{\partial r} \tag{3}$$

in the radial direction, assuming that the eddy is large enough that the centripetal force may be neglected [$\overline{u}_\theta/(fr) \ll 1$]. Here, F_z is the azimuthal-mean vertical flux of azimuthal wave momentum, also known as the Eliassen–Palm (EP) flux,

$$F_z = \overline{u'_\theta u'_z} + \frac{\overline{fu'_r b'}}{N^2}, \tag{4}$$

where primes denote the wave component of the flow. The divergence of the radial flux of azimuthal momentum $\partial_r\overline{u'_\theta u'_r}$ has been neglected in Eq. (2), as have all fluxes of radial momentum in Eq. (3), consistent with our deduction above that they will be zero for an isotropic wave field and zero radial flow in the eddy. From Eq. (2), the azimuthal-mean kinetic energy equation is obtained by multiplying by the velocity $\overline{u}_\theta$ and integrating in space

$$\frac{\partial K_\theta}{\partial t} = \frac{\partial}{\partial t}\left(\int_{-H}^{0}\int_0^\infty \frac{\overline{u}_\theta^2}{2} 2\pi r dr dz\right) = -\int_{-H}^{0}\int_0^\infty \overline{u}_\theta \frac{\partial F_z}{\partial z} 2\pi r dr dz \equiv W, \tag{5}$$

where W is the wave-to-mean conversion and $z = -H$ is the ocean bottom. For sufficiently small amplitude waves, the wave momentum flux F_z will be conserved (e.g., Eliassen 1962; Andrews and McIntyre 1976; Shakespeare and Hogg 2019) until (and unless) the waves encounter a critical level, at which point it is deposited into the flow. Since we do not know the exact profile of wave attenuation at a critical level, here we make the simplest approximation of instantaneous attenuation:

$$F_z(r, z) = \begin{cases} F_z^0, & -H \le z \le z_c(r) \\ 0, & \text{otherwise} \end{cases}, \tag{6}$$

where $z_c(r)$ denotes the location of the critical level and F_z^0 is the magnitude of the momentum flux below the critical level and eddy. In reality, we expect the wave attenuation to be smeared out over a finite height below the critical level; however, it is straightforward to show (see appendix) that this distinction does not significantly impact the wave-to-mean conversion as long as the wave attenuation height is small compared with the vertical scale of the eddy. Substituting Eq. (6) into Eq. (5) results in

$$W = \int_0^\infty \overline{u}_\theta|_c F_z^0 2\pi r dr, \tag{7}$$

where

$$\overline{u}_\theta|_c = \frac{\Omega - f}{k_\theta} \tag{8}$$

is the value of $\overline{u}_\theta$ at the critical level, as derived above [Eq. (1)]. At this point, it is convenient to relate the vertical momentum flux F_z^0 to the corresponding vertical energy flux E_z^0 outside of the eddy; the two are related through the phase speed (e.g., Booker and Bretherton 1967; Bretherton and Garrett 1968; Bretherton 1969; Bell 1975; Shakespeare 2020),

$$F_z^0 = \frac{k_\theta}{\Omega} E_z^0. \tag{9}$$

We emphasize that this relation [Eq. (9)] only applies where there is no mean flow and therefore no Doppler shift (otherwise, the Eulerian frequency Ω would need to be replaced by

[1] Here, the eddy considered is anticyclonic, but the same dynamics apply for cyclonic eddies.

intrinsic frequency ω); that is, it relates the wave energy and momentum fluxes (E_z^0, F_z^0) radiating from the topography, before the waves encounter the eddy. Substituting Eqs. (8) and (9) into Eq. (7), we have that

$$W = \left(1 - \frac{f}{\Omega}\right)\int_0^\infty E_z^0 2\pi r dr = \left(1 - \frac{f}{\Omega}\right)E, \tag{10}$$

where E is the total wave energy flux encountering the eddy (in waves for which a critical level exists). We can immediately observe from Eq. (10) that of this total energy, a fraction of $0 < 1 - f/\Omega \leq 1$ is transferred to the eddy. Assuming that there is no wave reflection or similar wave–wave energy exchange, the remainder of the energy in these waves that ultimately encounter critical levels (i.e., $E - W$) must be lost through either viscous dissipation ϵ_v or irreversible mixing ϕ_i as these are the only possible sinks in the wave energy budget (Müller 1976; Shakespeare and Hogg 2017a,b). The total dissipation $\epsilon = \epsilon_v + \phi_i$ in the eddy is therefore

$$\epsilon = \frac{f}{\Omega}E. \tag{11}$$

Thus, we predict that the partitioning of wave energy between energization and dissipation is independent of the wavenumber (albeit assuming that the wavenumber is large enough that a critical level exists).

In the next section, we use numerical simulations to verify the two key theoretical predictions made above: (i) there is a net acceleration of the eddy due to deposition of wave momentum [Eq. (5)] at critical levels and (ii) the wave energy flux into the eddy is partitioned into eddy energization and wave dissipation according to the wave frequency relative to the local inertial frequency [Eqs. (10) and (11)].

3. Numerical model

a. Model configuration

We use the MITgcm (Marshall et al. 1997) configured in the hydrostatic mode for a doubly periodic f-plane domain, 500 km in width and length, and 2 km in depth. The resolution is a uniform 500 m in the horizontal and 10 m in the vertical. Following Shakespeare et al. (2021a,b), a barotropic tide is generated by the addition of a barotropic body force $F_x = F_0 \sin\Omega t$ to the x-momentum equation, where F_0 is the amplitude and $\Omega = 2\pi/T$, where $T = 12$ h is the tidal period, which (in the absence of topography) drives a tidal flow of

$$u_t = F_0 \frac{\Omega}{f^2 - \Omega^2}\cos\Omega t, \quad v_t = -F_0 \frac{f}{f^2 - \Omega^2}\sin\Omega t. \tag{12}$$

We initialize the model with uniform stratification (buoyancy frequency N^2) and a Gaussian eddy (maximum buoyancy anomaly Δb) in the center of the domain; the initial buoyancy is

$$b = N^2 z + \Delta b e^{z/h}\exp\left(-\frac{r^2}{R^2}\right) \tag{13}$$

TABLE 1. Parameter values for the 12 simulations reported herein: tidal flow amplitude in the x direction u_t^0, background stratification N^2, inertial frequency f, and corresponding latitude ϕ. The buoyancy anomaly is adjusted according to $\Delta b/f = 48$ m s^{-1} to keep the eddy velocity [Eq. (14)] and Rossby number constant in all simulations. Also reported is the maximum horizontal wavelength for which a critical level exists, $\lambda_c = 2\pi/k_c$, where $k_c = (\Omega - f)/\max(u_\theta)$.

No.	Name	u_t^0 (cm s^{-1})	N^2 (10^{-5} s^{-2})	f (10^{-4} s^{-1})	ϕ (°N)	λ_c (km)
1	u_t	1.30	2	1	43.4	16.6
2	$2u_t$	2.61	2	1	43.4	16.6
3	$4u_t$	5.22	2	1	43.4	16.6
4	$8u_t$	10.4	2	1	43.4	16.6
5	$2N^2$	5.22	4	1	43.4	16.6
6	$N^2/2$	5.22	1	1	43.4	16.6
7	$1.05f$	10.4	2	1.39	72.2	109
8	$1.1f$	10.4	2	1.32	65.4	57.0
9	$1.2f$	10.4	2	1.21	56.4	31.1
10	$1.25f$	10.4	2	1.16	53.1	25.9
11	$1.35f$	10.4	2	1.08	47.8	20.0
12	$1.6f$	10.4	2	0.909	38.7	13.8

in geostrophic balance with a velocity field

$$u_\theta = \frac{-2rh\Delta b}{fR^2}e^{z/h}\exp\left(-\frac{r^2}{R^2}\right), \tag{14}$$

where $r^2 = x^2 + y^2$, noting that $x = y = 0$ is the domain center, and the Cartesian xy velocities are given by $(u, v) = u_\theta(-y/r, x/r)$. As in the previous section, we define the ocean surface as $z = 0$ and the ocean bottom as $z = -H$. We impose an eddy radius of $R = 100$ km and an eddy depth of $h = 300$ m; the other parameters vary between simulations (see Table 1). The total initial velocity field imposed in the model is the sum of the eddy velocity [Eq. (14)] and the tidal velocity [Eq. (12)] at time zero. The model determines the initial pressure through hydrostatic balance,

$$p = \rho_0\int_{-H}^{z} b\, dz, \tag{15}$$

and the corresponding free surface height (which we plot below) as $\eta = p(z = 0)/(\rho_0 g)$, where g is the acceleration due to gravity. The model is run with a Laplacian viscosity (i.e., diffusion of momentum) of $\nu_h = 10^{-2}$ m^2 s^{-1} in the horizontal and $\nu_v = 2 \times 10^{-4}$ m^2 s^{-1} in the vertical. The explicit horizontal and vertical diffusivities (of buoyancy) are set to zero. These choices minimize the anomalous destruction of the background stratification via vertical diffusion, while maintaining the stability of the model.

The bottom topography is constructed using an isotropic Goff (1991) abyssal hill spectrum defined by the power spectra

$$|\hat{h}|^2 = 4\pi h_{\text{rms}}^2 \frac{1}{K_c^2}\left(\frac{K^2}{K_c^2} + 1\right)^{-2}, \tag{16}$$

where $K = |\mathbf{k}_h|$ is the modulus of the horizontal wavenumber, $K_c = 10^{-4}$ m^{-1} is the corner wavenumber (corresponding to

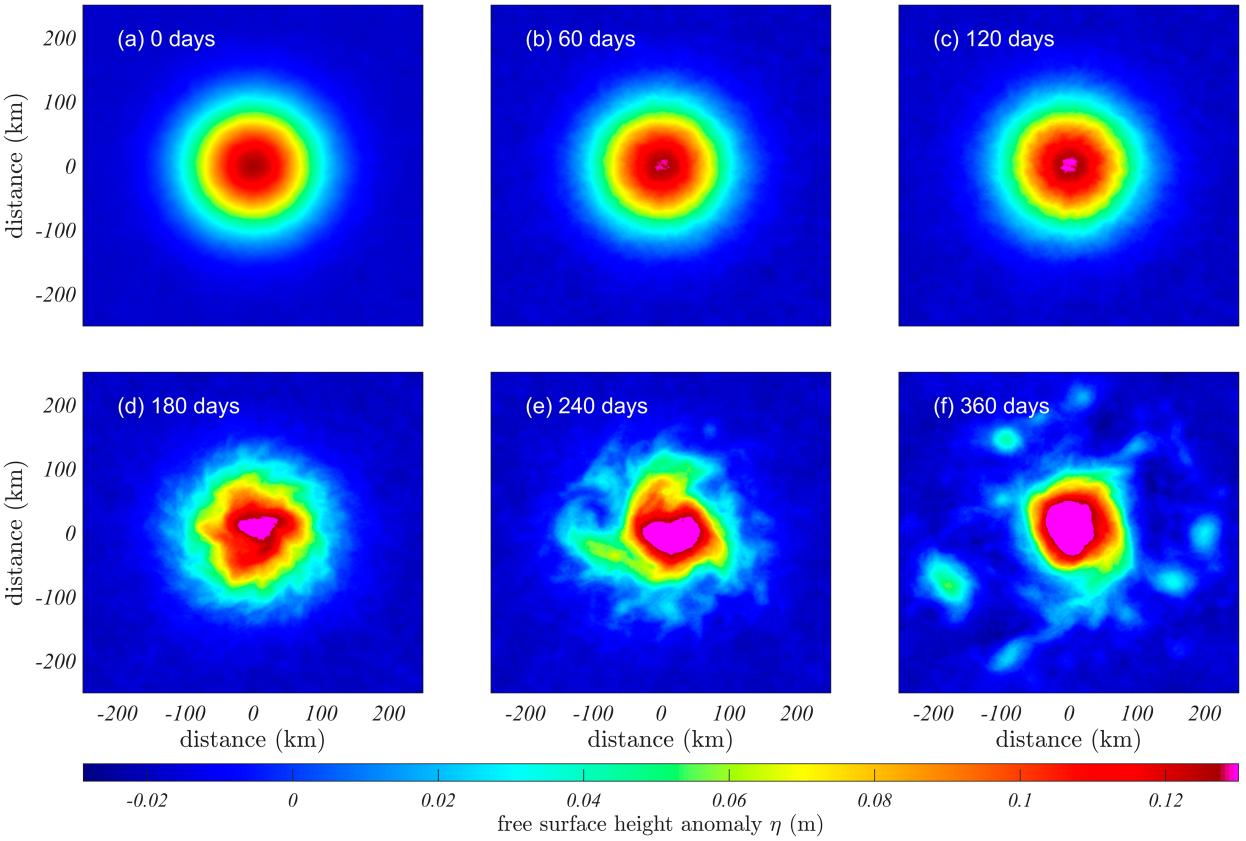

FIG. 3. Time evolution of the free surface height anomaly η in the $4u_t$ simulation (case 3 in Table 1). The eddy remains near-axisymmetric from (a) 0 to (b) 60 days as it is accelerated by the wave forcing (note the increase in maximum η in the eddy core; also see Fig. 4). At later times, (c) 120, (d) 180, and (e) 240 days, instabilities manifest as azimuthal variability and ultimately lead to the breakdown of the original eddy into smaller eddies and filaments by (f) 360 days.

wavelength $\lambda = 2\pi/K = 62$ km), and $h_{\rm rms} = 100$ m is the root-mean-square height of the topography. Further, we set the spectral amplitude to zero for wavelengths smaller than $\lambda = 2\pi/K = 5$ km to ensure that the topography is well resolved. Phases are randomly assigned, and an inverse Fourier transform is applied to generate the physical space topography from the spectral form [Eq. (16)].

A suite of 12 simulations is run (see Table 1) with varying tidal velocity, stratification, and inertial frequency. The eddy velocity is kept constant in all cases by adjusting the buoyancy anomaly Δb in proportion to the inertial frequency such that $\Delta b/f = 48$ m s^{-1}, corresponding to a fixed maximum Rossby number Ro = max$[f^{-1}(\partial u_\theta/\partial r)] = 0.056$—well within the geostrophic regime.

Time-averaged velocity fields, viscous dissipation ($\epsilon = \nu_h|\nabla_h \mathbf{u}|^2 + \nu_v|\partial_z \mathbf{u}|^2$), and momentum flux are output every 5 days (10 tidal cycles) of simulation. These output fields are then projected onto cylindrical coordinates (i.e., $x = r\cos\theta$, $y = r\sin\theta$) and averaged in θ to determine the azimuthal-mean velocity $\overline{u}_\theta$, momentum flux F_z [i.e., Eq. (4)], and dissipation. This momentum flux and dissipation will (initially and for some finite time thereafter) be entirely associated with internal waves, since they are the only source of radial and vertical velocities (which control the momentum flux) and the only source of sharp velocity gradients (which controls dissipation). It is then straightforward to compute the azimuthal-mean kinetic energy $\overline{u}_\theta^2/2$ and the conversion of wave energy into the azimuthal mean flow [i.e., $-\overline{u}_\theta \partial_z F_z$ as per Eq. (5)].

b. Analysis

Figure 3 shows the evolution of the free surface height anomaly for the $4u_t$ case (see Table 1) over the course of 360 days of simulation. The corresponding total azimuthal-mean kinetic energy (Fig. 4, black line) shows that the eddy accelerates over time, initially at a constant rate until ~120 days. The radial pressure gradient also increases to maintain geostrophic balance (as can be seen by the increase in free surface height in the core of the eddy in Fig. 3). Beyond ~120 days, radial perturbations grow and the initial eddy breaks down into smaller eddies and filaments (see Figs. 3d,e,f). The kinetic energy increases more rapidly during this phase due to the conversion of eddy available potential energy into kinetic energy. As expected, the acceleration rate of the eddy and time it breaks down depends on the strength of the wave forcing. Figure 4 shows the evolution of azimuthal-mean kinetic energy for four simulations with successive doublings of the tidal flow speed. For

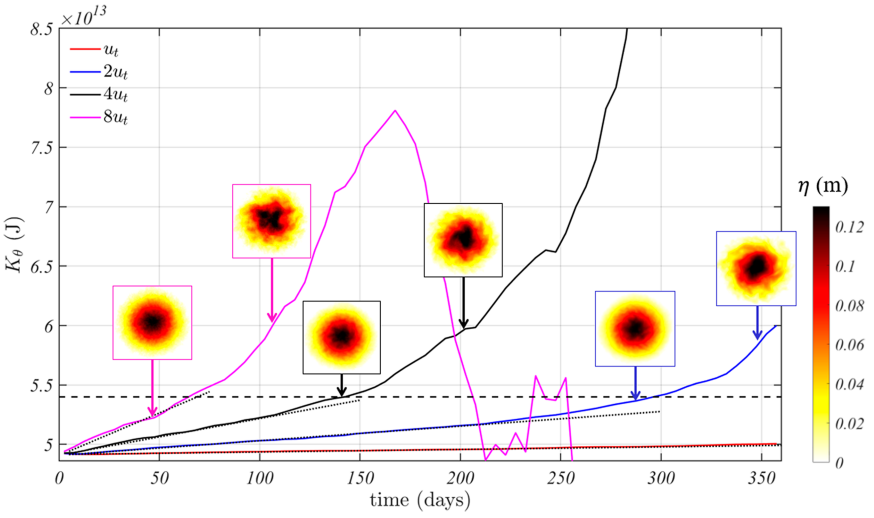

FIG. 4. Time evolution of the azimuthal-mean kinetic energy K_θ for four simulations with increasing tidal forcing: u_t, $2u_t$, $4u_t$, and $8u_t$ (see legend). All other parameters remain the same. The rate of increase in K_θ is constant initially, until the eddy breaks down for $K_\theta \sim 5.5 \times 10^{13}$ J (dashed line). The dotted gray lines show the linear trend over this initial period; the magnitude of the trends initially increases approximately quadratically with tidal forcing (for u_t, $2u_t$) but more slowly at larger forcing ($4u_t$, $8u_t$) due to the increasingly nonlinearity of the wave field near the topography. At later times, the flow field is no longer near axisymmetric and the behavior of K_θ thus becomes erratic. The breakdown of the eddy is illustrated by contour plots of free surface height anomaly η just before $K_\theta \sim 5.5 \times 10^{13}$ J and 60 days later.

the weaker forcing (red and blue), the eddy remains stable—and the K_θ increases at a constant (slower) rate—for significantly longer (beyond 1 year for the weakest forcing case), whereas the eddy breaks down after only 75 days for the largest flow speed ($8u_t$, magenta), but at the same kinetic energy level ($\sim 5.5 \times 10^{13}$ J) as for the $4u_t$ case. Here, our focus is on the initial constant acceleration phase.

Figure 5 displays the azimuthal-mean flow, dissipation, and wave-to-mean conversion for the same simulation shown in Fig. 3, averaged over days 25–30. Relative to the values outside the eddy, the dissipation in the core is enhanced by a factor of ~10 (Fig. 5b), consistent with internal waves encountering a critical level at this location. The wave-to-mean conversion W is also large in this region, but with compensating positive and negative signals (Fig. 5c). To determine where the net wave-to-mean conversion occurs, we sum W (and dissipation) over contours of azimuthal mean velocity—starting at the maximum (surface) value of $\overline{u}_\theta$—to produce the dashed lines shown in Fig. 5d. We also compute the mean dissipation rate along each $\overline{u}_\theta$ contour (Fig. 5d; purple). This analysis illustrates that there is a significant positive wave-to-mean conversion that occurs entirely within the eddy ($u_\theta > 0.02$ m s^{-1}) and predominantly in the core of the eddy ($u_\theta > 0.07$ m s^{-1}) where the dissipation is largest. The total wave-to-mean conversion accurately predicts the acceleration of the eddy during the initial linear phase (Fig. 5e).

Unlike the wave-to-mean conversion, the dissipation summed over $\overline{u}_\theta$ contours continues to increase beyond the bounds of the eddy due to the background wave dissipation (Fig. 5d; dashed red line). Thus, in order to determine the amount of dissipation occurring *within the eddy*—and therefore associated with the wave-to-mean conversion at critical levels—it is necessary to choose a velocity threshold defining the boundary of the eddy. Here, we take this threshold as the $\overline{u}_\theta$ value for which the dissipation rate is minimum: $\overline{u}_\theta = 0.02$ m s^{-1}, indicated by the vertical dashed line in Fig. 5d. This minimum occurs because internal waves at the edge of the eddy are being channeled into the eddy core by its flow field, thus depleting the wave energy (and dissipation) at the periphery relative to the background values. The minima in the dissipation rate are consistent at $\overline{u}_\theta = 0.02$ m s^{-1} across all our simulations (not shown) and will be used throughout our subsequent analysis to define the dissipation within the eddy. As for the wave-to-mean conversion, the total dissipation within the eddy remains constant for some initial period of time (i.e., the time-integrated dissipation shown by the dashed red line in Fig. 5e has a constant slope).

We compute the time-mean eddy acceleration $\partial_t K_\theta$, wave-to-mean conversion W, and dissipation within the eddy ϵ over the first 75 days of each simulation (which ensures that we remain in the linear phase for even the most extreme forcing cases). The uncertainty in these values is estimated by repeating the calculation over only days 50–75 of the simulation and taking the difference. Figure 6a shows that the acceleration of the eddy ($\partial_t K_\theta$) is generally well predicted by the wave-to-mean conversion W, as expected from the theory [Eq. (5)]. In Fig. 6b, we plot the acceleration $\partial_t K_\theta$ as a function of the total wave energy flux into the eddy ($E = W + \epsilon$) for the six cases with fixed inertial frequency. The results are consistent with the theoretical prediction [Eq. (10)] that $\partial_t K_\theta = (1 - f/\Omega)E = 0.31E$ (indicated by the dashed black line).

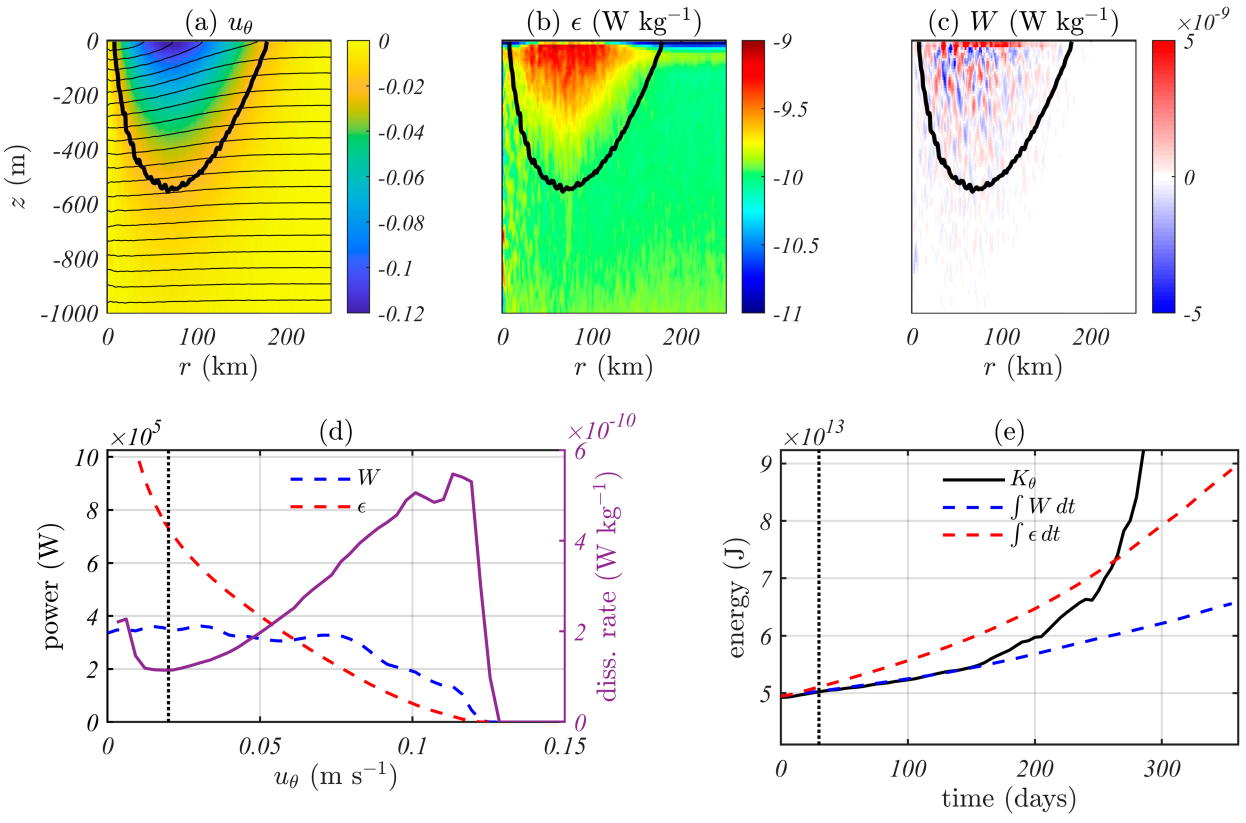

FIG. 5. Azimuthal-mean fields for the $4u_t$ simulation (number 3 in Table 1). (a) Mean azimuthal velocity, (b) energy dissipation, and (c) wave-to-mean energy conversion, averaged over days 25–30 of the simulation. The thin black lines in (a) are isotherms. The thick black line in (a)–(c) is the $\overline{u}_\theta = 0.02$ m s^{-1} contour. (d) Energy conversion and dissipation summed over $\overline{u}_\theta$ contours. Dashed lines (left axis) are the total power of the wave-to-mean conversion and dissipation between the surface and a given value of $|\overline{u}_\theta|$. The solid purple line (right axis) is the average dissipation rate on a given $\overline{u}_\theta$ contour. The vertical dashed line at $\overline{u}_\theta = 0.02$ m s^{-1} identifies the minimum dissipation rate. (e) Time evolution of the azimuthal-mean kinetic energy K_θ, time-integrated total dissipation $\int \epsilon\,dt$ within the eddy (i.e., for $\overline{u}_\theta > 0.02$ m s^{-1}), and time-integrated total wave-to-mean conversion $\int W\,dt$. The vertical dashed line indicates the time (30 days) to which plots (a)–(d) correspond.

Figure 6c displays wave-to-mean energy flux relative to the total wave energy flux into the eddy ($\partial_t K_\theta/E$) for the six simulations spanning a range of inertial frequencies (latitudes), but with consistent tidal forcing. The wave-to-mean fraction is broadly consistent with our prediction [Eq. (10)]; it is smallest for near-inertial frequencies (low latitudes) and increases monotonically as the frequency becomes more superinertial (higher latitudes). In general, the theory slightly underestimates the fraction at lower frequencies ($\Omega < 1.5f$) and slightly overestimates at higher frequencies ($\Omega > 1.5f$). Here, we have restricted our analysis to $f < \Omega \leq 1.6f$ to avoid the parametric subharmonic instability that manifests in the wave field near $\Omega = 2f$ (e.g., MacKinnon et al. 2013) and thereby complicates the analysis.

4. Discussion

We have shown that internal tide generation at abyssal hills leads to acceleration of ocean mesoscale eddies through the decay of the waves at critical levels within the eddies. Only waves traveling (and carrying momentum) in the direction of the local eddy flow encounter a critical level (Fig. 2), and therefore, the momentum deposited upon wave decay acts to accelerate the eddy. Here, we have developed theory to describe the wave dissipation and wave-to-mean energy exchange occurring during this process and verified the theory by comparison with a suite of idealized numerical simulations.

The importance of this mechanism in the global ocean is governed by two competing effects. First, the existence of a critical level requires that the speed of an eddy $u > (\Omega - f)/k$ for wave frequency Ω and wavenumber k. Thus, critical levels are ubiquitous at near-inertial frequencies but become less common at more superinertial frequencies. Second, we have shown that energy carried by a wave encountering a critical level is partitioned such that a fraction $1 - f/\Omega$ accelerates the eddy, while the remaining f/Ω is associated with dissipation and mixing. Thus, the more near-inertial a wave is, the less of its energy contributes to accelerating the eddy. It follows that this mechanism will be most effective at accelerating eddies at intermediate values of Ω/f. Thus, the mechanism will be

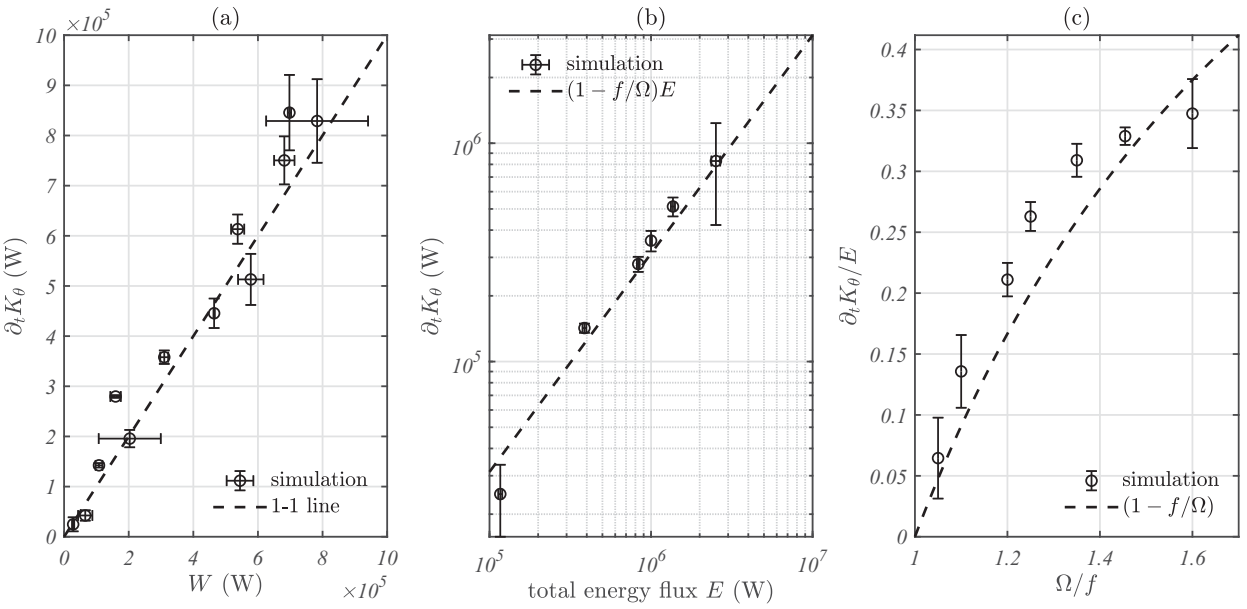

FIG. 6. Evaluation of theoretical predictions for all 12 simulations reported herein. (a) Comparison of the eddy acceleration $\partial_t K_\theta$ with the wave-to-mean conversion W, which are predicted to be equal [i.e., Eq. (5); dashed line]. (b) The eddy acceleration $\partial_t K_\theta$ plotted with respect to the total energy flux into the eddy $E = W + \epsilon$ for the six simulations with $f = 10^{-4}$ s^{-1}. These are predicted to scale as per the dashed black line [i.e., $\partial_t K_\theta = 0.31E$, Eq. (10)]. (c) The fraction of the energy flux accelerating the eddy $\partial_t K_\theta / E$ with respect to frequency Ω/f for the six simulations with varying f. The theoretical prediction [Eq. (10)] is shown as a dashed black line. In each plot, the error bars are calculated as the difference between time averages of quantities taken over (i) 0–75 and (ii) 50–75 days of simulation.

effective for mid-to-high-latitude semidiurnal internal tides (as studied in the present work) but ineffective for other types of internal waves, e.g., near-inertial wind-generated waves.

Let us consider some specific numbers. For a typical abyssal hill wavelength of ~15 km at a latitude of ~50°, we require velocities exceeding 8 cm s^{-1} for the existence of a critical level. Such velocities are ubiquitous in the intensely eddying currents—the Gulf Stream and Antarctic Circumpolar Current—that occupy these latitudes in both hemispheres. In addition, there is a significant semidiurnal internal tide energy flux (of ~1–10 mW m^{-2}; see Fig. 9 of Shakespeare 2020) from abyssal hills at these latitudes in the North Atlantic and in the Atlantic and Pacific sectors of the Southern Ocean. Based on the latitude and frequency, we expect approximately $1 - f/\Omega = 23\%$ of this energy flux to contribute to eddy acceleration, which equates to ~0.23–2.3 mW m^{-2}. Typical eddy kinetic energy (i.e., $\rho_0|\mathbf{u}|^2/2$) in these regions is in the range 25–100 J m^{-3} at the surface (e.g., Martínez-Moreno et al. 2021) which equates to ~12.5–50 kJ m^{-2}, assuming a 500-m e-folding depth for the eddy velocity. Taking the upper limit of each estimate, we predict an acceleration rate of

$$\frac{2.3\,\text{mW m}^{-2}}{50\,\text{kJ m}^{-2}}(86\,400\,\text{s day}^{-1}) = 0.4\%\ \text{day}^{-1},$$

or 12% month^{-1}. Given mesoscale eddies have typical lifetimes of many months, this effect would therefore represent a very significant contribution to their energy and life cycle. Recall that in our simulations, a ~10% amplification of the eddy by waves (see Fig. 4) was sufficient to trigger its instability and breakdown. Thus, our calculations suggest that internal tides may play a key role in both eddy energization and their subsequent instability and decay. Increased eddy instability would tend to offset the enhanced eddy kinetic energy in a time and space mean, since it would lead to more intense, but fewer eddies.

It is useful to compare our calculations with previous simulations and observations of wave–eddy interactions. The mechanism of internal tide–driven eddy acceleration described here was previously suggested by Shakespeare and Hogg (2019), but the complexity of their simulations prevented a direct evaluation of the effect. Nonetheless, their simulations showed that realistic-amplitude internal tides at abyssal hill scales were able to amplify eddy vorticity by up to 44% (corresponding to a kinetic energy increase of $\sim 0.44^2 = 20\%$). Mooring observations in the Scotia Sea—directly in the path of the Antarctic Circumpolar Current—by Cusack et al. (2020) also support the mechanism described here. Cusack et al. (2020) report a net energy transfer of 2.2 ± 0.6 mW m^{-2} from internal waves to mesoscale eddies, a large fraction (~50%) of which occurs in the upper ocean and at the semidiurnal frequency. Furthermore, the wave-to-eddy energy exchange occurs almost entirely through the wave-driven vertical flux of horizontal momentum (i.e., $-u\partial_z F_z$), the same term implicated in the present work. These studies therefore further support our hypothesis that eddy energization by internal tides is an important process in the global oceans.

Unfortunately, internal wave generation at abyssal hills is too small to be resolved in most global ocean models and must be parameterized. Heretofore, parameterization of lee

wave drag and mixing has been investigated (Yang et al. 2021; Trossman et al. 2013, 2016), but internal tides have only been considered in the context of mixing (usually through a background effective diffusivity), with no consideration given to their ability to energize eddying circulation. Our results provide a pathway toward a more sophisticated parameterization for internal tides by prescribing the partitioning of energy between dissipation/mixing and wave-to-mean conversion.

Such a parameterization appears increasingly important to develop and implement in the context of ocean changes such as the persistent increase in eddy kinetic energy over the past three decades (Martínez-Moreno et al. 2021). Furthermore, recent work by Mak et al. (2022) has implicated the time scale of mesoscale eddy decay as a key parameter controlling the strength of the Antarctic Circumpolar Current and meridional overturning circulation. Reduced eddy decay time scales due to internal tides energizing eddies and thereby accelerating the onset of hydrodynamic instabilities—as observed in the present simulations—may therefore significantly influence these large-scale circulations. Parameterization of internal tide momentum transfer in global models will be crucial in further investigating these dynamics—a topic we leave for future work.

Acknowledgments. The author acknowledges funding from the Australian Research Council Discovery Project DP230101836. The author thanks A. Hogg and O. Bühler for helpful comments on an earlier draft of the manuscript.

Data availability statement. The numerical model simulations reported here are too large to archive in an accessible way, but we provide all the information needed to replicate the simulations: the edited model code, MATLAB code to generate input files, and the namelist settings are available at https://github.com/CallumJShakespeare/MITgcm_eddy_acceleration.

APPENDIX

The Profile of Wave Attenuation at Critical Levels

In the main text, we made the assumption [Eq. (6)] that waves attenuated instantaneously at critical levels. As noted therein, a more realistic model is that the waves attenuate over a region of finite height below the critical level. To investigate the impact of this more gradual attenuation, here we replace the instantaneous attenuation [Eq. (6)] with a piecewise linear form,

$$F_z(r, z) = \begin{cases} F_z^0, & -H \le z \le z_c - \Delta z \\ F_z^0 \dfrac{z_c - z}{\Delta z}, & z_c - \Delta z < z \le z_c, \\ 0, & \text{otherwise} \end{cases} \tag{A1}$$

implying a constant attenuation rate $F_z^0/\Delta z$ over a region of height Δz below the critical level z_c. Substituting Eq. (A1) into Eq. (5), the wave-to-mean conversion may be calculated as

$$W = \int_0^\infty \int_{z_c - \Delta z}^{z_c} \overline{u}_\theta \frac{F_z^0}{\Delta z} dz\, 2\pi r\, dr. \tag{A2}$$

We will now assume that the eddy velocity profile is exponential (as implemented in our numerical model) such that we may write

$$\overline{u}_\theta = \overline{u}_\theta|_c \exp\left(\frac{z - z_c}{h}\right), \tag{A3}$$

where h is the eddy e-folding depth (300 m in our simulations). The vertical integral in Eq. (A2) may then be evaluated to yield

$$\begin{aligned} W &= \int_0^\infty \overline{u}_\theta|_c F_z^0 (1 - e^{-\Delta z/h}) \frac{h}{\Delta z} 2\pi r\, dr, \\ &\simeq \int_0^\infty \overline{u}_\theta|_c F_z^0 \left(1 - \frac{\Delta z}{2h}\right) 2\pi r\, dr, \end{aligned} \tag{A4}$$

where we have taken the first-order expansion in $\Delta z/h$. Equation (A4) implies that a finite wave attenuation region reduces the wave-to-mean conversion by a fraction $\Delta z/(2h)$ due to the decreasing eddy flow speed with depth. In general, the attenuation height will depend on wave frequency, stratification, horizontal wavenumber, and fluid viscosity, making it challenging to calculate for an arbitrary wave field. However, as long as the attenuation height of waves Δz is small compared to the height scale of the eddy h, then the finite height may be neglected and instantaneous wave attenuation (as assumed in the main text) is a good approximation. In our numerical model, for example, the attenuation scale will primarily be determined by the distance from the critical level at which the vertical scale of the waves has reduced sufficiently for the vertical viscosity to act (since the model does not have sufficient resolution to directly resolve wave breaking). Thus, at minimum, Δz must be some small multiple of the model resolution (10 m). If we estimate $\Delta z \sim 60$ m, then we expect to introduce an error of $\Delta z/(2h) = 60/600$ or around 10% in our calculations where instantaneous attenuation has been assumed.

REFERENCES

Andrews, D. G., and M. E. McIntyre, 1976: Planetary waves in horizontal and vertical shear: The generalized Eliassen–Palm relation and the mean zonal acceleration. *J. Atmos. Sci.*, **33**, 2031–2048, https://doi.org/10.1175/1520-0469(1976)033<2031:PWIHAV>2.0.CO;2.

Baldwin, M. P., and Coauthors, 2001: The quasi-biennial oscillation. *Rev. Geophys.*, **39**, 179–229, https://doi.org/10.1029/1999RG000073.

Bell, T. H., Jr., 1975: Topographically generated internal waves in the open ocean. *J. Geophys. Res.*, **80**, 320–327, https://doi.org/10.1029/JC080i003p00320.

Booker, J. R., and F. P. Bretherton, 1967: The critical layer for internal gravity waves in a shear flow. *J. Fluid Mech.*, **27**, 513–539, https://doi.org/10.1017/S0022112067000515.

Bretherton, F. P., 1969: Momentum transport by gravity waves. *Quart. J. Roy. Meteor. Soc.*, **95**, 213–243, https://doi.org/10.1002/qj.49709540402.

——, and C. J. R. Garrett, 1968: Wavetrains in inhomogeneous moving media. *Proc. Roy. Soc. London*, **302A**, 529–554, https://doi.org/10.1098/rspa.1968.0034.

Cusack, J. M., J. A. Brearley, A. C. Naveira Garabato, D. A. Smeed, K. L. Polzin, N. Velzeboer, and C. J. Shakespeare, 2020: Observed eddy–internal wave interactions in the southern ocean. *J. Phys. Oceanogr.*, **50**, 3043–3062, https://doi.org/10.1175/JPO-D-20-0001.1.

Eliassen, A., 1962: On the vertical circulation in frontal zones. *Geofys. Publ.*, **24** (4), 147–160.

Ferrari, R., and C. Wunsch, 2009: Ocean circulation kinetic energy: Reservoirs, sources, and sinks. *Annu. Rev. Fluid Mech.*, **41**, 253–282, https://doi.org/10.1146/annurev.fluid.40.111406.102139.

Garrett, C., and W. Munk, 1975: Space-time scales of internal waves: A progress report. *J. Geophys. Res.*, **80**, 291–297, https://doi.org/10.1029/JC080i003p00291.

Goff, J. A., 1991: A global and regional stochastic analysis of near-ridge abyssal hill morphology. *J. Geophys. Res.*, **96**, 21 713–21 737, https://doi.org/10.1029/91JB02275.

Jones, W. L., 1967: Propagation of internal gravity waves in fluids with shear flow and rotation. *J. Fluid Mech.*, **30**, 439–448, https://doi.org/10.1017/S0022112067001521.

MacKinnon, J. A., M. H. Alford, O. Sun, R. Pinkel, Z. Zhao, and J. Klymak, 2013: Parametric subharmonic instability of the internal tide at 29°N. *J. Phys. Oceanogr.*, **43**, 17–28, https://doi.org/10.1175/JPO-D-11-0108.1.

Mak, J., D. P. Marshall, G. Madec, and J. R. Maddison, 2022: Acute sensitivity of global ocean circulation and heat content to eddy energy dissipation timescale. *Geophys. Res. Lett.*, **49**, e2021GL097259, https://doi.org/10.1029/2021GL097259.

Marshall, J., A. Adcroft, C. Hill, L. Perelman, and C. Heisey, 1997: A finite-volume, incompressible Navier Stokes model for studies of the ocean on parallel computers. *J. Geophys. Res.*, **102**, 5753–5766, https://doi.org/10.1029/96JC02775.

Martínez-Moreno, J., A. M. Hogg, M. H. England, N. C. Constantinou, A. E. Kiss, and A. K. Morrison, 2021: Global changes in oceanic mesoscale currents over the satellite altimetry record. *Nat. Climate Change*, **11**, 397–403, https://doi.org/10.1038/s41558-021-01006-9.

McIntyre, M. E., 1981: On the 'wave momentum' myth. *J. Fluid Mech.*, **106**, 331–347, https://doi.org/10.1017/S0022112081001626.

Muench, J. E., and E. Kunze, 2000: Internal wave interactions with equatorial deep jets. Part II: Acceleration of the jets. *J. Phys. Oceanogr.*, **30**, 2099–2110, https://doi.org/10.1175/1520-0485(2000)030<2099:IWIWED>2.0.CO;2.

Müller, P., 1976: On the diffusion of momentum and mass by internal gravity waves. *J. Fluid Mech.*, **77**, 789–823, https://doi.org/10.1017/S0022112076002899.

Plumb, R. A., 1977: The interaction of two internal waves with the mean flow: Implications for the theory of the quasi-biennial oscillation. *J. Atmos. Sci.*, **34**, 1847–1858, https://doi.org/10.1175/1520-0469(1977)034<1847:TIOTIW>2.0.CO;2.

——, and A. D. McEwan, 1978: The instability of a forced standing wave in a viscous stratified fluid: A laboratory analogue of the quasi-biennial oscillation. *J. Atmos. Sci.*, **35**, 1827–1839, https://doi.org/10.1175/1520-0469(1978)035<1827:TIOAFS>2.0.CO;2.

Rintoul, S. R., 2018: The global influence of localized dynamics in the southern ocean. *Nature*, **558**, 209–218, https://doi.org/10.1038/s41586-018-0182-3.

Shakespeare, C. J., 2020: Interdependence of internal tide and lee wave generation at abyssal hills: Global calculations. *J. Phys. Oceanogr.*, **50**, 655–677, https://doi.org/10.1175/JPO-D-19-0179.1.

——, and A. M. Hogg, 2017a: Spontaneous surface generation and interior amplification of internal waves in a regional-scale ocean model. *J. Phys. Oceanogr.*, **47**, 811–826, https://doi.org/10.1175/JPO-D-16-0188.1.

——, and ——, 2017b: The viscous lee wave problem and its implications for ocean modelling. *Ocean Modell.*, **113**, 22–29, https://doi.org/10.1016/j.ocemod.2017.03.006.

——, and ——, 2019: On the momentum flux of internal tides. *J. Phys. Oceanogr.*, **49**, 993–1013, https://doi.org/10.1175/JPO-D-18-0165.1.

——, B. K. Arbic, and A. McC. Hogg, 2021a: Dissipating and reflecting internal waves. *J. Phys. Oceanogr.*, **51**, 2517–2531, https://doi.org/10.1175/JPO-D-20-0261.1.

——, ——, and ——, 2021b: The impact of abyssal hill roughness on the benthic tide. *J. Adv. Model. Earth Syst.*, **13**, e2020MS002376, https://doi.org/10.1029/2020MS002376.

Trossman, D. S., B. K. Arbic, S. T. Garner, J. A. Goff, S. R. Jayne, E. J. Metzger, and A. J. Wallcraft, 2013: Impact of parameterized lee wave drag on the energy budget of an eddying global ocean model. *Ocean Modell.*, **72**, 119–142, https://doi.org/10.1016/j.ocemod.2013.08.006.

——, ——, J. G. Richman, S. T. Garner, S. R. Jayne, and A. J. Wallcraft, 2016: Impact of topographic internal lee wave drag on an eddying global ocean model. *Ocean Modell.*, **97**, 109–128, https://doi.org/10.1016/j.ocemod.2015.10.013.

Wunsch, C., and R. Ferrari, 2004: Vertical mixing, energy and the general circulation of the oceans. *Annu. Rev. Fluid Mech.*, **36**, 281–314, https://doi.org/10.1146/annurev.fluid.36.050802.122121.

Xie, J.-H., and J. Vanneste, 2017: Interaction between mountain waves and shear flow in an inertial layer. *J. Fluid Mech.*, **816**, 352–380, https://doi.org/10.1017/jfm.2017.39.

Yang, L., M. Nikurashin, A. McC. Hogg, and B. M. Sloyan, 2021: The impact of lee waves on the southern ocean circulation. *J. Phys. Oceanogr.*, **51**, 2933–2950, https://doi.org/10.1175/JPO-D-20-0263.1.